Photodiagnosis and Photodynamic Therapy 26 (2019) 90–96

Contents lists available at ScienceDirect

Photodiagnosis and Photodynamic Therapy

journal homepage: www.elsevier.com/locate/pdpdt

Mueller matrix imaging of prostate bulk tissues; Polarization parameters as a discriminating benchmark

Saeedesadat Badieyan[a,b], Ali Ameri[b], Mohammad Reza Razzaghi[a], Hashem Rafii-Tabar[b], Pezhman Sasanpour[b,*]

[a] Laser Application in Medical Sciences Research Center, Shahid Beheshti University of Medical Sciences, Tehran, Iran
[b] Department of Medical Physics and Biomedical Engineering, School of Medicine, Shahid Beheshti University of Medical Sciences, Tehran, Iran

ARTICLE INFO

Keywords:
Polarimetry imaging
Mueller matrix
Prostate tissue
Cancer detection

ABSTRACT

The polarimetry imaging technique has provided a powerful tool for discriminating normal from cancerous tissues. In this paper, based on the backscattering Mueller matrix imaging of prostate bulk tissues, (received immediately after surgery without any further processing), we have extracted the characteristic features of the Mueller matrix images. In order to provide a quantitative and more accurate comparison, three different methods have been used; the Mueller matrix polar decomposition (MMPD), the Mueller matrix transformation (MMT) and the frequency distribution histograms (FDHs) and their central moment parameters. Comparing different tissues, the results of our study indicate that these methods provide the indicators for the characteristics of the microstructural features of the tissues. The indicators have the potential to distinguish between cancerous and healthy tissues. Determining the polarimetric characteristics of the tissue immediately after surgery and prior to the pathology, and the potential possibility of this technique to be used in vivo as an optical biopsy technique, can significantly reduce the cost and time of diagnosis of cancer.

1. Introduction

Prostate cancer is the third leading cause of cancer death in men in the United States. It is estimated that 26,730 deaths from this disease will occur in 2018 [1]. Most often, cancers could be treated successfully if they are detected in the early stages. The 5-year survival rate for most of the men with local or regional prostate cancer is almost 100% and for the men diagnosed with prostate cancer that has spread to other parts of the body, is 29%. These statistics show that rapid and timely detection of local disease could greatly reduce the mortality rate of the prostate cancer [1–4]. Because of the importance of detecting cancer at early stages, global efforts and initiatives are on the rise, and several approaches have been proposed so far, each of which, depending on the cost, time, reliability and ease of use and the degree of discomfort for the patient.

One of the most accurate and widely used methods for detecting cancerous tissues is biopsy. Biopsy techniques have disadvantages, including cost, long-time detection and invasiveness. In addition, even with the advent of equipped laboratories, it is not possible to detect some of the cancers in the early stages through biopsy. The probability of detecting prostate cancer in the early stages with biopsy is about 70% [5,6].To improve the biopsy technique, a number of optical methods have been employed, e.g. Optical Coherence Tomography (OCT) [7,8], Photo-Acoustic Tomography (PAT) [9], Near-Infrared Spectroscopy (NIRS) [10], nonlinear microscopy [11], and confocal microscopy [12]. It should be mentioned that, due to the complexity of the tissue structures, these techniques have their own set of problems, for example, providing high resolution images is a time consuming process. To overcome these limitations, improved novel imaging and diagnosis techniques are required [5,13].

The use of polarization-based optical techniques has received considerable attention due to their ability for noninvasive scanning of tissues while providing additional information. The techniques provide valuable information that cannot be obtained directly from intensity or spectral images in various fields. This information is especially useful also for examination and diagnosis of surgically removed cancerous tumor tissues [5,14–27]. In order to have a non-invasive approach, polarimetry imaging as a low cost and rapid technique, has the potential to provide valuable information about bulky tissues. By exploiting optical fibers, the technique could be applied in-vivo and will help the physicians to find the margins of the cancerous tissue accordingly.

* Corresponding author.
E-mail address: pesasanpour@sbmu.ac.ir (P. Sasanpour).

https://doi.org/10.1016/j.pdpdt.2019.02.017
Received 26 November 2018; Received in revised form 13 February 2019; Accepted 19 February 2019
Available online 20 February 2019
1572-1000/

In a cancerous tissue, morphological changes occur that alter the polarization properties of the tissue. These different optical properties between healthy and abnormal tissues provide the ability to distinguish between cancerous and healthy tissues with the polarimetric method [14].

The 16 elements of the Mueller matrix provide the most general and complete description of microstructural and optical properties of a medium based on its ability to alter the polarization state [14,28–32]. But, since this information is qualitative, for a more accurate and quantitative examination, a number of methods are used. The Mueller matrix polar decomposition (MMPD) method that decomposes the complicated interactions between the polarized light and the sample into a series of polarization sensitive processes, and derives the corresponding polarization optical parameters, such as retardance, diattenuation, polarization and depolarization. The Mueller matrix transformation (MMT) is another method that by using 9 linear Mueller matrix elements provides valuable parameters. These methods provide groups of quantitative polarization parameters as a measure of polarimetric comparison between healthy and cancerous tissues [28,33–36].

In addition to the results obtained from the analysis of the Muller matrix for the comparison of tissues, another method is to use the Frequency Distribution Histogram (FDH) method and the central moment parameters derived from these diagrams. The data and parameters obtained from this statistical method, which are representative of the dominant features of the tissue, are orientation insensitive which is of a great advantage [37,38].

There has been some studies on the polarimetry imaging of human and dog prostate samples [39,40]. Based on the importance of the early detection of prostate cancer tissue in a noninvasive method, in this paper we have investigated the relatively important quantitative parameters of both polarization (MMPD) and the Mueller matrix transformation (MMT) and also the central moment's parameters derived from the full 4×4 Mueller matrix measurements. The preliminary results show that these valuable optical and structural information provided by the Mueller matrix of samples, may serve as criteria for discriminating cancer from normal prostate tissues.

2. Materials and methods

2.1. Experimental setup

In order to acquire images for different polarization states, we have established the Mueller matrix polarization imaging system which is schematically shown in Fig. 1. A laser diode (wavelength = 632.8 nm) was used as a light source. Generated coherent light produced by laser is passed from a polarization state generator (PSG), consisting of a linear polarizer and a quarter wave retarder to produce the arbitrary state of polarization of irradiation. At the input branch, a beam expander is used to provide uniform intensity illumination. After light interaction with the sample, the reflected light from the sample passes through the polarization state analyzer (PSA) unit, which has the same optical elements of the PSG assembled in reverse order. The resulting image of the sample falls on a CCD camera. To avoid the surface reflection of the sample, for all the measurements the angle between the input and the output branches is kept at 30°. Before real sample experiments, the setup is calibrated by measuring the Mueller matrix of standard samples with known Mueller matrices such as the linear polarizer. The calculated error for all the Mueller matrix elements was less than 3%.

2.2. Data analysis

The raw images were imported into the Matlab and the initial process including the noise cancellation and segmentation were performed on the raw images. The Mueller matrix is a mathematical representation, based on intensity measurements. Based on the equations

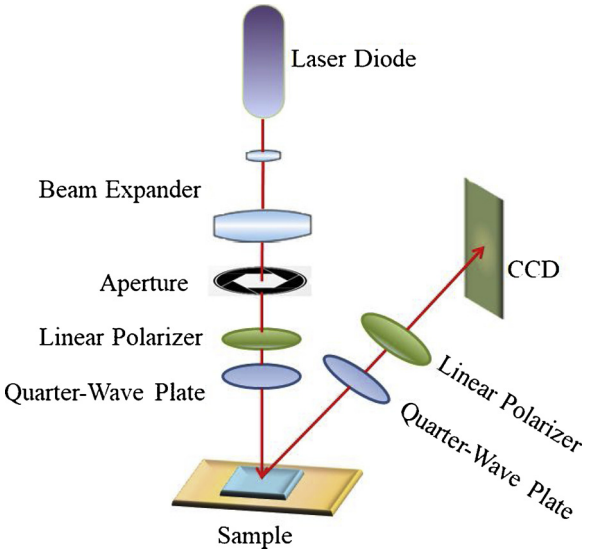

Fig. 1. The schematic setup of the Mueller matrix imaging system.

listed in Table 1 for the input and output light polarization states, all elements of the Mueller matrix could be calculated [41].The first term shows the input light polarization and the second term shows the output light polarization state. H and V represent horizontal and vertical. P and M indicate -45° and -45° linear state of polarization. R and L show the right circular and the left circular polarization. All the calculations for the imported images in addition to basic processing were performed based on our own code in the Matlab environment.

2.3. Analysis of polarimetric images

Although the Mueller matrix contains abundant valuable optical and structural information about the tissues, this information is qualitative on the microstructures of the samples and often there is not a clear connection between the Mueller matrix elements and the optical and structural properties of the sample. In this regard, for a more accurate examination and comparison of tissues, quantitative analysis of the optical behavior of the samples are needed. The Mueller matrix polar decomposition (MMPD) proposed by Lu–Chipman is used to obtain optical parameters [33]. In the MMPD a Mueller matrix can be decomposed into three basic submatrices: the depolarizing matrix (M_Δ), the retardance matrix (M_R), and the diattenuation matrix (M_D) as stated by Eq. 1.

$$\boldsymbol{M} = \boldsymbol{M}_\Delta \boldsymbol{M}_R \boldsymbol{M}_D \tag{1}$$

Based on Eq. 1, a set of parameters are derived corresponding to these matrices; the diattenuation D can be calculated by Eq. 2, the polarizance P can be expressed in terms of the Mueller matrix of equation 3, the depolarization power Δ, can be obtained from Eq. 4 and the retardance R can be obtained by Eq. 5:

$$D = \frac{1}{m_{00}}\sqrt{m_{01}^2 + m_{02}^2 + m_{03}^2} \tag{2}$$

$$P = \frac{1}{m_{00}}\sqrt{m_{10}^2 + m_{20}^2 + m_{30}^2} \tag{3}$$

$$\Delta = 1 - \frac{|tr(M_\Delta) - 1|}{3} \tag{4}$$

$$R = cos^{-1}\left[\frac{tr(\boldsymbol{M}_R)}{2} - 1\right] \tag{5}$$

where "tr" expresses the trace of matrices.

Apart from the MMPD, some of the polarization parameters are derived from certain transformation process. New group of optical

Table 1
The Mueller matrix derivation equations.

$M_{11} = HH + HV + VH + VV$	$M_{12} = HH + HV - VH - VV$	$M_{13} = PH + PV - MH - MV$	$M_{14} = RH + RV - LH - LV$
$M_{21} = HH - HV + VH - VV$	$M_{22} = HH - HV - VH + VV$	$M_{23} = PH - PV - MH + MV$	$M_{24} = RH - RV - LH + LV$
$M_{31} = HP - HM + VP - VM$	$M_{32} = HP - HM - VP + VM$	$M_{33} = PP - PM - MP + MM$	$M_{34} = RP - RM - LP + LM$
$M_{41} = HR - HL + VR - VL$	$M_{42} = HR - HL - VR + VL$	$M_{43} = PR - PL - MR + ML$	$M_{44} = RR - RL - LR + LL$

parameters for quantitatively characterizing the properties of anisotropic scattering media by using the Mueller matrix transformation (MMT) technique are obtained using Eqs. 6–8([42]).

$$A = \frac{2b.\ t}{b^2 + t^2} \in [0,1] \tag{6}$$

$$b = \frac{m_{22} + m_{33}}{2} \tag{7}$$

$$t = \frac{\sqrt{(m_{22} - m_{33})^2 + (m_{23} + m_{32})^2}}{2} \tag{8}$$

The parameter t is sensitive to the anisotropic degree of scattering media. For an isotropic media t is equal zero. For an easier examination, by normalizing the parameter t, the new parameter A can be obtained. The parameter A shows the anisotropy degree and characterizes the order of alignment of the fibrous scatterers. Several properties such as the depolarization, absorption and birefringence, determine the value of the parameter b. However, for calculating the MMT parameters for bulk tissues with strong depolarization, the parameter b is mainly related to the depolarization ability [43].

In another method to quantitatively evaluate the Mueller matrix images, we have extracted the characteristic features of the Mueller matrix images based on the statistical method. In this method, the Mueller matrix images are transferred into the frequency distribution histogram (FDH), that shows the distribution of intensity for each of the pixels of the image, and central moment parameters. In this regard, each image of the Mueller matrix is adopted to the central moment method for converting to its FDH and the central moments for statistical analysis using Eqs. 9–12 [37,43,44].

$$Mean\ value = \mu = P1 = E(X) \tag{9}$$

$$Variance = \sigma^2 = P2 = E[(X - \mu)^2] = Var(X) \tag{10}$$

$$Skewness = \gamma = P3 = \frac{E(X - \mu)^2}{\sigma^2} \tag{11}$$

$$Kurtosis = Kurt[X] = P4 = \frac{E(X - \mu)^4}{\sigma^4} \tag{12}$$

2.4. Tissue samples

All procedures were performed in accordance with the Shahid Beheshti University of Medical Sciences ethical guidelines. Ethical approval (IR.SBMU.MSP.REC.1397.147) was obtained from the Research Ethics Committee of the School of Medicine, Shahid Beheshti University of Medical Sciences. The healthy and cancerous human prostate tissues were used as samples. One of the tissue samples is shown in Fig. 2. The tissue samples were received immediately after surgery form Shohada-e-Tajrish hospital in 10% formaldehyde solution and no cutting and the staining operation was performed on them. For each sample polarimetry imaging was performed immediately after surgery. The Mueller matrix was then generated for all samples and the important elements of the Mueller matrix were determined to be the indices to distinguish between the cancerous and healthy prostate tissues [31,43].

Fig. 2. A prostate tissue sample. The scale bar is 1 cm.

3. Results

Calibration of the system is done in order to ensure the accuracy of measurement system. The system is checked with the air and mirror as the samples. The error was calculated as the difference between the measured values (from the system) and the theoretical values for the air and mirror. The maximum of errors in the elements of matrix were not more than 3%.

Fig. 2 shows one of the prostate tissue sample that received immediately after surgery. Fig. 3 shows the calculated backscattering Mueller matrix images of healthy and cancerous prostate tissues. The normalized Mueller matrix is derived by dividing the elements of the Mueller matrix to the first element (m_{00}). Fig. 4 shows the normalized Mueller matrix images of the healthy and cancerous prostate tissues.

Using the Mueller matrix polar decomposition algorithm and by processing each pixel of images, the related polarization images including the diattenuation *D*, the depolarization power Δ, the polarizance P and the retardance R were calculated. Intensity images for the healthy and cancerous prostate tissues are presented in Fig. 5. Fig. 5a and e show the diattenuation images of the cancerous and healthy prostate tissues respectively. Figs. 5b and 5f show the depolarization images and Fig. 5c and g show the polarizance of cancerous and healthy prostate tissues. The retardance image of cancerous and healthy tissues are represented in Fig. 5d and h accordingly.

In order to have a quantitative and more precise criterion, Table 2 shows the value of each polarization parameter of cancerous and healthy prostate tissues. The parameters are all derived from the intensity images and equations [1–8]. First, the average intensity for each element of the Muller matrix is derived from the related image accordingly. Using this intensity value and through equations 2 to 5 for the MMPD (based on the method presented by Lu-Chipman) the values of the retardance, polarizance, depolarization and attenuation are calculated (Table 2). The values of A and b in Table 2 are derived using the intensities obtained for the elements of the Mueller matrix and equations 5 to 8.

Fig. 6 shows the frequency distribution histogram (FDH) of the Mueller matrix elements of the healthy prostate tissue (solid blue line) and the cancerous prostate tissue (dashed red line). The FDH for each element of matrix has been calculated using its own intensity image accordingly.

As it can be seen from Fig. 6, cancerous and healthy prostate tissues show different FDH distributions. Table 3 represents the calculated central moments for two samples.

4. Discussion

The complete Mueller matrix provides rich microstructural and optical information about the sample. The presence of both diagonal and non-diagonal elements of the Mueller matrix images, as seen from Figs. 3 and 4, confirms that both samples are anisotropic. Furthermore, the parameter b is related directly to the diagonal values of m22 and m33. Since the parameters b and depolarization power have negative correlation, the larger diagonal parameters values indicate a larger value for parameter b and a lower depolarization properties of sample

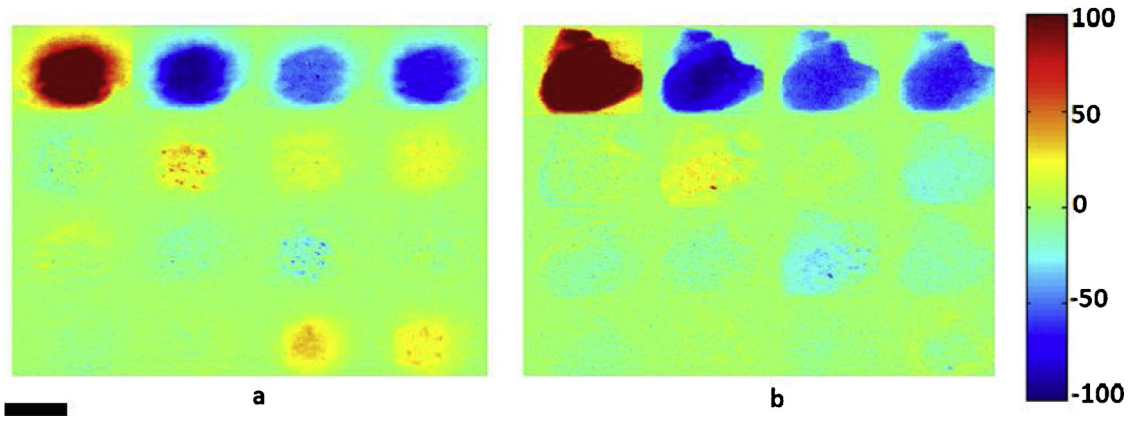

Fig. 3. Calculated backscattering Mueller matrix images of a) healthy prostate tissue, b) cancerous prostate tissue. The scale bar is 1 cm.

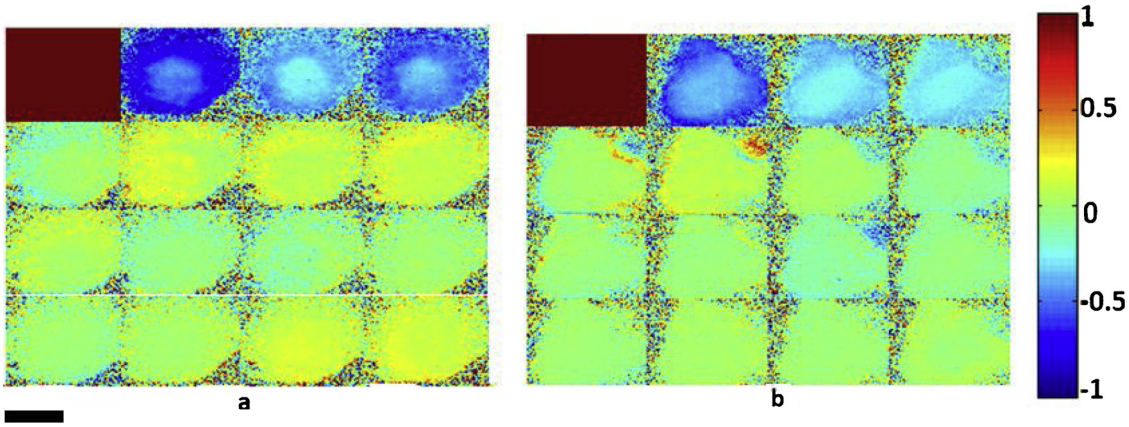

Fig. 4. Calculated backscattering normalized Mueller matrix images of a) healthy prostate tissue, b) cancerous prostate tissue. The scale bar is 1 cm.

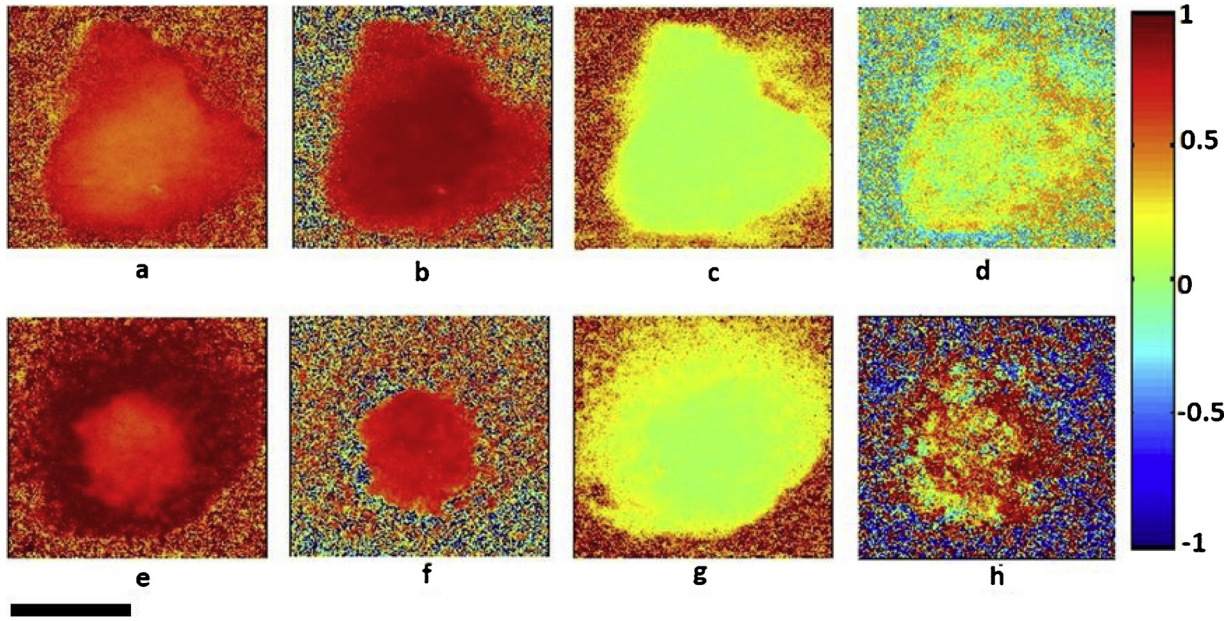

Fig. 5. Two dimensional intensity distribution of a) diattenuation, b) depolarization, c) polarizance and d) retardance for a cancerous prostate tissue and e) diattenuation, f) depolarization, g) polarizance and h) retardance for a healthy prostate tissue. The scale bar is 1 cm.

[43]. Based on the results of Figs. 3 & 4, it is confirmed that the depolarization in the cancerous tissue is larger than the healthy tissue, which can be due to the larger and denser cell nuclei in the cancerous tissues that act as scattering particles. Since the polarization values are close to each other, a qualitative comparison is not sufficient, therefore in order to address this problem and obtain more precise optical data to compare healthy and cancerous tissues, quantitative analysis of the Mueller matrix is required. The other advantages of quantitative values are the insensitivity of these parameters to the sample orientation. The MMPD, the MMT and central moments analysis methods are algorithms

Table 2
The values of optical parameters obtained for cancerous and healthy prostate tissues.

Polarization parameter	Samples	
	Cancerous prostate tissue	Healthy prostate tissue
Diattenuation	0.7419	0.7176
Depolarization	0.8864	0.8636
Polarizance	0.0893	0. 0452
Retardance	0.1648	0.5094
A	0.2050	0.3140
b	0.0955	0.1565

which are employed in this study to compare healthy and cancerous prostate tissues with a more quantitative measure.

By comparing images of Fig. 5 with the parameters of Table 2, more precise information for comparison between samples could be obtained. It can be observed from Fig. 5a, e and Table 2 that the cancer prostate tissue exhibits more diattenuation than the healthy one, but the difference is not significant. This result can be due to the rapid growth of the cancerous cells and their high density and the larger nucleus of the cancer cells compared with the healthy tissue which increases the absorption of light. Furthermore Fig. 5b, f and Table 2 show that the structure of the cancerous prostate tissue will cause more depolarization compared with the healthy one. Due to the negative correlation between depolarization feature and the parameter b, it is expected that with increasing the depolarization parameter (cancerous prostate tissue), the parameter b will decrease, which is confirmed in Table 2 [43]. Fig. 5c, g and Table 2 confirm that microstructural variations due to cancer could increase the polarizance of the cancerous tissue. Considering Fig. 5d, h and Table 2, it can be concluded that the retardance and the parameter A for the cancerous tissue have decreased in comparison with the healthy tissue. It is because of this fact that the fibrous structure of tissues in the healthy tissues, is a highly organized structure and strongly anisotropic compared with the cancerous tissues. The rapid growth of the cancerous cells reduces the order of alignment of the fibers and as a result there would be lower anisotropy in the structure. Therefore, the value of A and the tissue retardation value are reduced in cancerous tissues.

Fig. 6 shows the frequency distribution histogram (FDH) of the Mueller matrix elements of the cancerous and the healthy prostate tissues. Fig. 6 demonstrates different FDH curves for healthy and cancerous tissues due to different structural and characteristic features. Table 3 shows the parameters P1, P2, P3 and P4 which are calculated central moments of the Mueller matrix elements for normal and abnormal prostate tissues. The shapes of the FDHs and their central

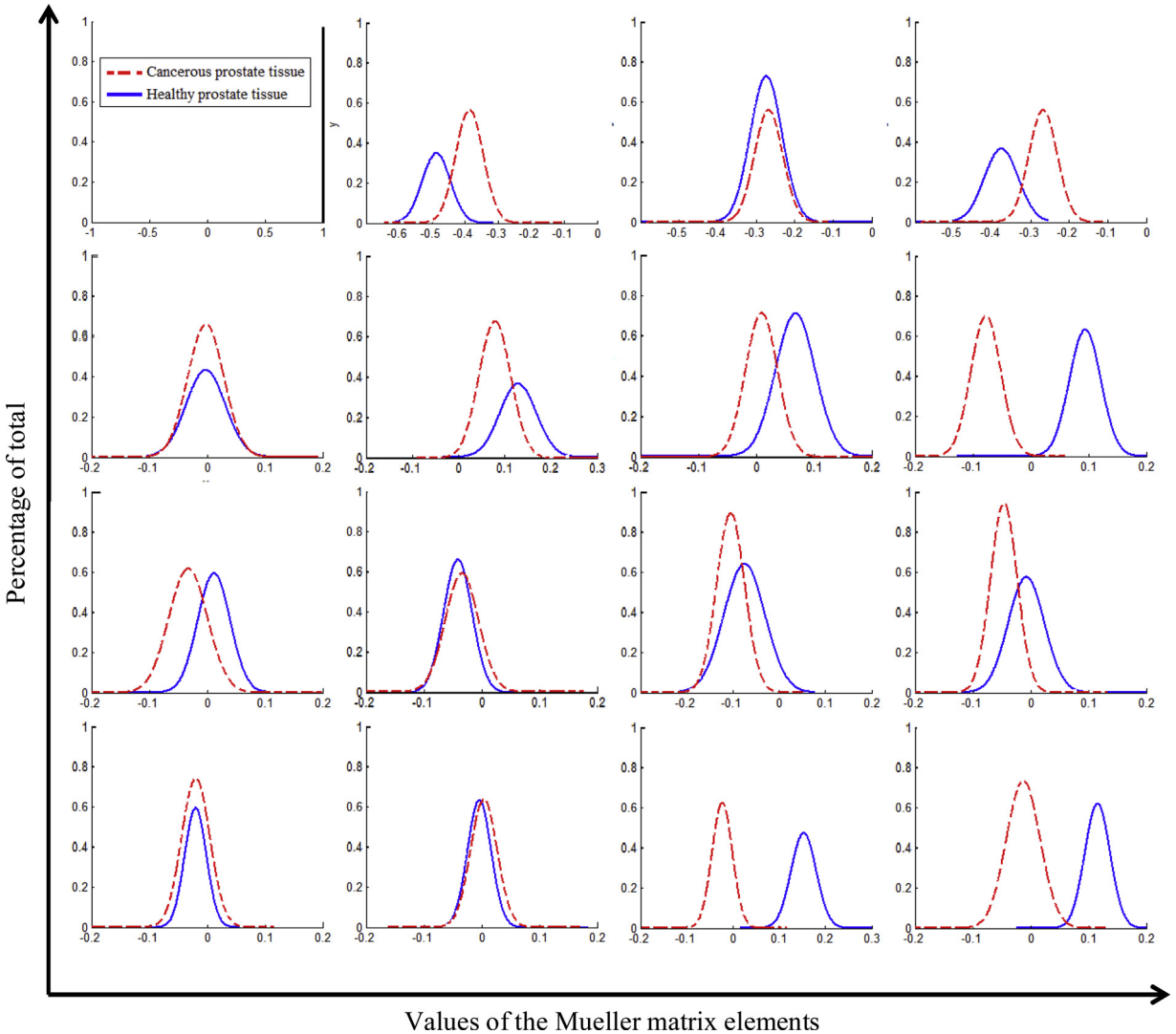

Fig. 6. Frequency distribution histogram (FDH) of the Mueller matrix elements of a cancerous prostate tissue (dashed red line) and a healthy prostate tissue (solid blue line). The areas under the curves are normalized to 1.

Table 3
The central moment parameters of the Mueller matrix elements for human prostate cancerous and healthy tissues.

	m12	m13	m14	m21	m22	m23	m24	m31	m32	m33	m34	m41	m42	m43	m44
abnormal/P1	−0.391	−0.271	−0.274	−0.001	0.0804	0.0096	−0.077	−0.033	−0.034	−0.105	−0.046	−0.018	0.0056	0.023	−0.008
normal/P1	−0.487	−0.274	−0.378	−0.007	0.1332	0.066	0.0946	0.0136	−0.042	−0.079	−0.008	−0.02	−0.004	0.1526	0.1173
abnormal/P2	0.0306	0.0191	0.0076	0.0032	0.0752	0.00098	0.0025	0.0074	0.0023	0.1245	0.001	0.0012	0.0011	0.0011	0.017
normal/P2	0.0074	0.0462	0.0236	0.0109	0.0397	0.0392	0.0068	0.0046	0.0045	0.297	0.0096	0.001	0.0011	0.0028	0.0019
abnormal/P3	0.8729	−0.265	−1.587	−0.919	1.9207	0.1735	−2.516	−0.04	−0.304	−1.922	−1.375	−1.991	0.6463	−0.993	−2.441
normal/P3	−0.401	0.8452	−0.679	−0.354	0.6592	0.1026	−0.568	−1.179	1.0918	−1.575	−0.416	−0.901	1.2604	−0.787	0.4596
abnormal/P4	8.2824	7.3172	6.3715	8.3887	8.6865	3.4803	6.8295	5.2179	5.3223	9.0893	7.1792	8.0245	5.4549	4.3957	4.2961
normal/P4	6.3784	8.9582	2.8976	7.4387	5.3243	4.567	3.8511	7.8738	5.4371	10.787	2.6597	3.8208	6.4466	2.5807	4.4334

moments values provide more precise quantitative optical characteristic information to distinguish between the normal and abnormal prostate tissues.

The increasing differences between m22 and m33 (diagonal curves) correspond to the increasing of anisotropy of sample. [37]. Based on Fig. 6 and Table 3, the difference in P1 between m22 and m33 for the normal tissue is more than the abnormal tissue which shows that the healthy prostate tissue is more anisotropic than the cancerous one. As mentioned before, this anisotropy is a direct result of presence of more aligned fibers in healthy tissue than the cancerous one. The larger values of the first central moment (P1) for the diagonal value of the backscattered Mueller matrix samples show the smaller depolarization power and vice versa [37]. Therefore, based on Fig. 6 and Table 3, it can be concluded that cancerous tissue has more depolarization power than the healthy one, while this result is consistent with those previously obtained from Table 2 and Fig. 5d and f. The second central moment (P2) indicates that how far each measured intensity values for every elements of normalized Mueller matrix are from the mean value. For larger P2, the FDHcurves have larger width, which implies that there is more complexity in the sample. The results of Table 3 show somehow the same value of P2 for abnormal and normal tissues. The negligible differences indicate that the cancerous tissue is more complex than the healthy tissue, which can be due to the uncontrolled proliferation of cancerous cells. The positive and negative values of P1 for m34 and m43 are an indicator that could be applied to compare the birefringence effect in the normal and abnormal tissues. As seen in Table 3, this difference for abnormal prostate tissue is less than the normal tissues which expresses that the birefringence effect for abnormal tissue is limited. Considering Table 3, P3 (skewness) and P4 (kurtosis) for some Mueller matrix elements have significant differences in values that can be used as indicators for the heterogeneity and complexity respectively [37]. To determine more accurately the relationship between these parameters and microstructue of the tissues more study is required.

5. Conclusion

In this study based on the backscattering Mueller matrix imaging, the polarization properties of the cancerous and healthy bulk prostate tissues have been studied. The tissues were imaged immediately after surgery without any cutting and staining. Compared with the standard H-E staining method, the technique can be used as a rapid and less costly method, while it has the potential to be applied in vivo through the endoscopic techniques. To reduce the probability of errors and increase the accuracy, each sample was imaged several times and the average results were used. The Mueller matrix of samples provide the qualitative comparison between healthy and cancerous prostate tissues. In order to provide more accurate, quantitative parameters MMPD, MMT techniques and the FDHs and their central moments analysis are used for quantitative comparison between the polarization properties of the cancerous and the healthy prostate tissues. The preliminary results of our study show that the methods (the Muller matrix images, the MMPD, the MMT and the FDHs and their central moments) provide good quantitative indicators of the microstructures of tissues that may have the potential to distinguish between the cancerous and healthy prostate tissues. The retardance value for the MMPD and the parameter A for the MMT, are more powerful characteristics for differentiation between the healthy tissue and the cancer tissue.

Author's contributions

P.S. conceived the project and with the contribution of S.B., the optical set up of experiments, image processing and data analysis were performed. M.R.R provided the samples and contributed in analysis of data. S.B. and P.S. performed the experiments, analyzed the results and wrote the manuscript. H.R-T., M.R.R. and A.A. provided advice, expertise, and all authors read and edited the manuscript.

Competing interest

We declare we have no competing interests.

Acknowledgements

The present article is financially supported by "Laser Applications in Medical Sciences Research Center" of Shahid Beheshti Medical University (Grant No. 13304).

References

[1] R.L. Siegel, K.D. Miller, A. Jemal, Cancer statistics, 2018, CA Cancer J. Clin. 68 (1) (2018) 7–30.
[2] https://www.cancer.net/cancer-types/prostate-cancer/statistics [.
[3] https://www.cancer.org/content/dam/CRC/PDF/Public/8793.00.pdf.
[4] J.D. Wulfkuhle, L.A. Liotta, E.F. Petricoin, Early detection: proteomic applications for the early detection of cancer, Nat. Rev. Cancer 3 (4) (2003) 267.
[5] B. Kunnen, C. Macdonald, A. Doronin, S. Jacques, M. Eccles, I. Meglinski, Application of circularly polarized light for non-invasive diagnosis of cancerous tissues and turbid tissue-like scattering media, J. Biophotonics 8 (4) (2015) 317–323.
[6] O.M. Zaytoun, J.S. Jones, Prostate cancer detection after a negative prostate biopsy: lessons learnt in the Cleveland Clinic experience, Int. J. Urol. 18 (8) (2011) 557–568.
[7] M.E. Brezinski, G.J. Tearney, B.E. Bouma, J.A. Izatt, M.R. Hee, E.A. Swanson, et al., Optical coherence tomography for optical biopsy: properties and demonstration of vascular pathology, Circulation 93 (6) (1996) 1206–1213.
[8] B.G. Muller, D.M. Bruin, M.J. Brandt, W. Bos, S. Huystee, D. Faber, et al., Prostate cancer diagnosis by optical coherence tomography: first results from a needle based optical platform for tissue sampling, J. Biophotonics 9 (5) (2016) 490–498.
[9] P. Beard, Biomedical Photoacoustic Imaging, Interface focus, 2011 rsfs20110028.
[10] J. Ali, W. Wang, M. Zevallos, R. Alfano, Near infrared spectroscopy and imaging to probe differences in water content in normal and cancer human prostate tissues, Technol. Cancer Res. Treat. 3 (5) (2004) 491–497.
[11] A.M. Garcia, F.L. Magalhes, J.S. Soares, E.P. Junior, M.F. de Lima, M. Mamede, et al., Second harmonic generation imaging of the collagen architecture in prostate cancer tissue, Biomed. Phys. Eng. Express 4 (2) (2018) 025026.
[12] I.V. Tereshchenko, H. Zhong, M.A. Chekmareva, N. Kane-Goldsmith, U. Santanam, W. Petrosky, et al., ERG and CHD1 heterogeneity in prostate cancer: use of confocal microscopy in assessment of microscopic foci, Prostate 74 (15) (2014) 1551–1559.
[13] T. Novikova, A. Pierangelo, A. De Martino, A. Benali, P. Validire, Polarimetric imaging for cancer diagnosis and staging, Opt. Photonics News 23 (10) (2012) 26–33.
[14] N. Ghosh, A.I. Vitkin, Tissue polarimetry: concepts, challenges, applications, and outlook, J. Biomed. Opt. 16 (11) (2011) 110801.

[15] N. Ghosh, M.F. Wood, Li Sh, R.D. Weisel, B.C. Wilson, R.K. Li, et al., Mueller matrix decomposition for polarized light assessment of biological tissues, J. Biophotonics 2 (3) (2009) 145–156.
[16] F. Fanjul-Vélez, N. Ortega-Quijano, J.L. Arce-Diego, Polarimetry group theory analysis in biological tissue phantoms by Mueller coherency matrix, Opt. Commun. 283 (22) (2010) 4525–4530.
[17] M.F. Wood, N. Ghosh, E.H. Moriyama, B.C. Wilson, I.A. Vitkin, Proof-of-principle demonstration of a Mueller matrix decomposition method for polarized light tissue characterization in vivo, J. Biomed. Opt. 14 (1) (2009) 014029.
[18] S. Firdous, M. Atif, M. Nawaz, Study of Blood Malignancy in Vitro for the Diagnosis and Treatment of Blood Diseases Using Polarimetery and Microscopy 19 Lasers in Engineering (Old City Publishing), 2010.
[19] N. Ghosh, M.F. Wood, I.A. Vitkin, Influence of the order of the constituent basis matrices on the Mueller matrix decomposition-derived polarization parameters in complex turbid media such as biological tissues, Opt. Commun. 283 (6) (2010) 1200–1208.
[20] L. Qiu, D.K. Pleskow, R. Chuttani, E. Vitkin, J. Leyden, N. Ozden, et al., Multispectral scanning during endoscopy guides biopsy of dysplasia in Barrett's esophagus, Nat. Med. 16 (5) (2010) 603.
[21] Mueller polarimetry for the detection of cancers, in: E. Du, H. He, N. Zeng, Y. Guo, M. Sun, H. Ma, et al. (Eds.), Advanced Biomedical and Clinical Diagnostic Systems XII, International Society for Optics and Photonics, 2014.
[22] J.F. De Boer, T.E. Milner, Review of polarization sensitive optical coherence tomography and Stokes vector determination, J. Biomed. Opt. 7 (3) (2002) 359–372.
[23] A.H. Hielscher, J.R. Mourant, I.J. Bigio, Influence of particle size and concentration on the diffuse backscattering of polarized light from tissue phantoms and biological cell suspensions, Appl. Opt. 36 (1) (1997) 125–135.
[24] A. Doronin, C. Macdonald, I.V. Meglinski, Propagation of coherent polarized light in turbid highly scattering medium, J. Biomed. Opt. 19 (2) (2014) 025005.
[25] X. Feng, R. Patel, A.N. Yaroslavsky, Wavelength optimized cross-polarized wide--field imaging for noninvasive and rapid evaluation of dermal structures, J. Biophotonics 8 (4) (2015) 324–331.
[26] S. Alali, A. Kim, N. Vurgun, M.F. Wood, I.A. Vitkin, M. Ahmad, Quantitative correlation between light depolarization and transport albedo of various porcine tissues, J. Biomed. Opt. 17 (4) (2012) 045004.
[27] A. Pierangelo, A. Benali, M.-R. Antonelli, T. Novikova, P. Validire, B. Gayet, et al., Ex-vivo characterization of human colon cancer by Mueller polarimetric imaging, Opt. Express 19 (2) (2011) 1582–1593.
[28] R. Chipman, Polarimetry, Chapter 22, Editor in Chief, in: M. Bass (Ed.), Handbook of Optics, vol 2, 1994, p. 37.
[29] C. Brosseau, Fundamentals of Polarized Light: a Statistical Optics Approach, Wiley-Interscience, 1998.
[30] S.A. Hall, M.-A. Hoyle, J.S. Post, D.K. Hore, Combined stokes vector and Mueller matrix polarimetry for materials characterization, Anal. Chem. 85 (15) (2013) 7613–7619.
[31] E. Du, H. He, N. Zeng, M. Sun, Y. Guo, J. Wu, et al., Mueller matrix polarimetry for differentiating characteristic features of cancerous tissues, J. Biomed. Opt. 19 (7) (2014) 076013.
[32] A. Vitkin, M. Wood, N. Ghosh, Polarized light assessment of complex turbid media such as biological tissues Us-ing mueller matrix decomposition, Handbook of Photonics for Biomedical Science, CRC Press, 2010, pp. 284–313.
[33] S.-Y. Lu, R.A. Chipman, Interpretation of Mueller matrices based on polar decomposition, JOSA A 13 (5) (1996) 1106–1113.
[34] J. Chung, W. Jung, M.J. Hammer-Wilson, P. Wilder-Smith, Z. Chen, Use of polar decomposition for the diagnosis of oral precancer, Appl. Opt. 46 (15) (2007) 3038–3045.
[35] Transformation of full 4× 4 Mueller matrices: a quantitative technique for biomedical diagnosis, in: H. He, J. Chang, C. He, H. Ma (Eds.), Dynamics and Fluctuations in Biomedical Photonics XIII, International Society for Optics and Photonics, 2016.
[36] P. Shukla, A. Pradhan, Mueller decomposition images for cervical tissue: potential for discriminating normal and dysplastic states, Opt. Express 17 (3) (2009) 1600–1609.
[37] C. He, H. He, X. Li, J. Chang, Y. Wang, S. Liu, et al., Quantitatively differentiating microstructures of tissues by frequency distributions of Mueller matrix images, J. Biomed. Opt. 20 (10) (2015) 105009.
[38] Y. Dong, H. He, C. He, J. Zhou, N. Zeng, H. Ma, Characterizing the effects of washing by different detergents on the wavelength-scale microstructures of silk samples using Mueller matrix polarimetry, Int. J. Mol. Sci. 17 (8) (2016) 1301.
[39] Stokes polarimetry imaging of dog prostate tissue, in: J. Kim, W.K. Johnston, J.T. Walsh (Eds.), Photonic Therapeutics and Diagnostics VI, International Society for Optics and Photonics, 2010.
[40] Statistical and fractal approaches in laser polarimetry diagnostics of the cancer prostate tissues, in: A. Ushenko, S. Yermolenko, A. Prydij, S. Guminetsky, I. Gruia, O. Toma, et al. (Eds.), Eighth International Conference on Correlation Optics (2008).
[41] B.D. Cameron, M. Raković, M. Mehrübeoğlu, G.W. Kattawar, S. Rastegar, L.V. Wang, et al., Measurement and calculation of the two-dimensional backscattering Mueller matrix of a turbid medium, Opt. Lett. 23 (7) (1998) 485–487.
[42] H. He, N. Zeng, E. Du, Y. Guo, D. Li, R. Liao, et al., A possible quantitative Mueller matrix transformation technique for anisotropic scattering media/Eine mögliche quantitative Müller-Matrix-Transformations-Technik für anisotrope streuende Medien, Photonics Lasers Med. 2 (2) (2013) 129–137.
[43] M. Sun, H. He, N. Zeng, E. Du, Y. Guo, S. Liu, et al., Characterizing the microstructures of biological tissues using Mueller matrix and transformed polarization parameters, Biomed. Opt. Express 5 (12) (2014) 4223–4234.
[44] O. Toma, E. Dinescu, Application of the matrix formalism in a Mueller matrix imaging polarimetry, Rom. Rep. Phys. 60 (4) (2008) 1065–1070.